Journal of Power Sources, 50 (1994) 109–120

The meniscus cell
Part I. Experimental

Juhani Kivisaari* and Olle Lindström
Royal Institute of Technology, Department of Chemical Technology, 100 44 Stockholm (Sweden)

(Received November 13, 1992; in revised form November 22, 1993; accepted November 27, 1993)

Abstract

A new method for quick screening of gas-diffusion electrodes has been developed. The method may also be suitable for the evaluation of the diffusion characteristics of the catalyst layer of a hydrophobic gas-diffusion electrode. The electrodes are stepwise immersed in the electrolyte. The current is generated in the meniscus zone of the electrode where electrolyte and gas meet. These studies were performed with cathodes catalyzed with silver or pyrolyzed cobalt-tetramethoxyphenylporphyrine fed with pure oxygen and mixtures with 20.0, 5.0 and 1.0% oxygen in nitrogen. The results from the measurements imply that the current–voltage curves depend on the depth-of-immersion (DOI) and that the cell could be used for quality control in electrode preparation. A figure-of-merit is derived from the data obtained with the meniscus cell. This figure is a measure of the mass-transfer characteristics of the catalyst layer. The slope of the current–voltage curve for deeply immersed electrodes is another figure-of-merit, which is obtained in a most straightforward way.

Background and objectives

Grove's fuel cell was a meniscus cell with the electrolyte meniscus climbing up along black platinum wires. Our version is not really different. A strip of a modern gas-diffusion electrode is immersed in the electrolyte surrounded by the reactant gas, e.g., air with the counter electrode in the electrolyte beaker. A reference electrode is placed close to the surface of the partially immersed gas-diffusion electrode.

This simple setup is useful for screening electrode formulations. The meniscus cell may, however, provide more information than figures-of-merit for screening purposes. The experimental conditions can be varied in a controlled manner to give data which throw some light on the mass-transfer characteristics of the electrode. The depth-of-immersion, DOI, is such a parameter.

The initial purpose of the meniscus cell was to simulate the conditions in the catalyst layer in the air cathodes of a novel iron/air cell [1, 2]. This concept, called '041', gives a high-energy density because of minimized cell pitch, Fig. 1. Oxygen and electrolyte contact the electrode from the same side. The air electrode is separated from the iron electrode by a conducting polymer sheet serving as a bipolar collector. The meniscus cell simulates the reaction zone in this particular cell concept.

*Author to whom correspondence should be addressed.

0378-7753/94/$07.00
SSDI 0378-7753(93)01890-T

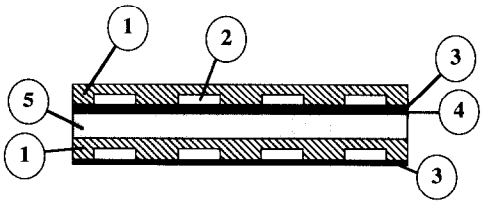

Fig. 1. Electrode arrangement according to the '041' concept: (1) separator soaked with electrolyte (5 M KOH); (2) air channel; (3) catalyst layer of air electrode; (4) gas-tight conductive polymer sheet, and (5) iron electrode.

The mass-transport pattern of most fuel cell electrodes may be described as 'straight on' since the processes are going on 'in and out' perpendicular to the electrode surface. There are, however, notable exceptions. The present molten carbonate fuel cell (MCFC) concepts could be described as 'around the corner', since reactants and reaction products have to make a turn in the electrode material after passing through the holes of the current collector. The '041' configuration also exhibits an 'around the corner' flow pattern.

Experiments with the meniscus cell may give information about the processes in the electrode layer in the shielded electrode parts and data for optimization of the geometry of the separator, in particular the width of the separator rib.

The meniscus cell is useful for screening electrode formulations in a cost-efficient manner, which is a primary objective of the present work. The current–voltage curve for a partially immersed electrode is such a straightforward screening parameter. The test cell consists simply of a beaker with a holder for the electrode. The curve obtained should be related to the current–voltage curve for a conventional cell and not only to the '041' design described above. Increased immersion should give successively smaller contributions to the total current.

Björnbom [3] has developed a mathematical model for the current distribution, concentration gradients, etc., for the '041' configuration. The simulation results suggest that it may be difficult to obtain high-power density with the '041' concept due to the *IR* drop in the part of the cathode under the gas channel. No firm conclusions could be drawn from these model studies, however, since data for effective gas diffusivity in the catalyst layer under the separator ribs were lacking. The meniscus experiments provide experimental evidence regarding the load characteristics of these zones.

In experiments with partially immersed electrodes, the electrode potential should be fairly uniform throughout the catalyst layer at low-current densities because of the high conductivity of the electrode structure and the small dimensions. This feature should simplify the interpretation of the data obtained in these tests.

A second objective of this work is to develop a method for evaluation of the gas-diffusion characteristics of the catalyst layer. The reactant gas travels down as much as about 5 mm in the meniscus zone of the electrode shown in Fig. 2. Polarization is then caused mainly by mass-transfer limitations in the catalyst layer of the electrode.

The present approach is apparently somewhat related to Will's [4] studies of the electrochemical oxidation of hydrogen on partially immersed platinum-wire electrodes. Kaisheva *et al.* [5] used a similar method to study immersed air electrodes for zinc/air batteries. Here, the electrodes were furnished with a thick gas-diffusion layer, in which the oxygen travelled down. The oxygen then had to diffuse only a short way through the catalyst layer, Fig. 3.

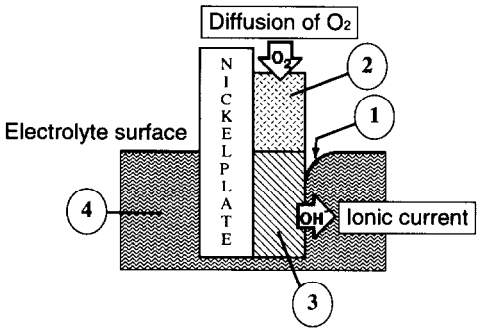

Fig. 2. Diffusion patterns in a meniscus electrode: (1) meniscus downward in contact with the hydrophobic surface; (2) gas-diffusion layer of porous PTFE; (3) catalyst layer, and (4) electrolyte (5 M KOH).

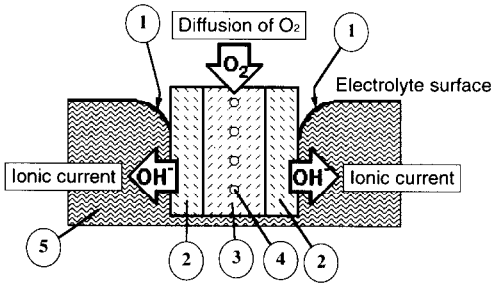

Fig. 3. Electrode according to Kaisheva *et al.* [5]: (1) meniscus; (2) catalyst layer; (3) diffusion layer; (4) current collector grid, and (5) electrolyte (5 M KOH).

In the present approach, on the other hand, the oxygen has to travel down in the catalyst layer itself, which is likely to give more relevant information about electrode characteristics.

A meniscus electrode arrangement has also been used in an oxygen sensor and was invented by Hersch [6, 7]. Hersch's oxygen analyser consists of two conductive electrodes. preferably silver wire, with a non-conducting porous diaphragm in between and in contact with them. The diaphragm is tubular and filled with an aqueous electrolyte such as 5 M KOH. The wires are coiled in a double helix around the tubular diaphragm. An external electrical voltage, sufficient to cathodically reduce the oxygen, but insufficient to electrolyse water, is applied during use, and the current measured for the oxygen assay. The electrode reactions are here reduction of oxygen on the cathode and formation of silver oxide on the anode.

Hersch's analyser is thus in a sense a silver/air cell with meniscus electrodes.

Experimental

Test cell

The cell is a rectangular vessel made of polycarbonate connected to a piston burette, Fig. 4. The electrolyte level in the cell is raised in steps by addition of electrolyte from the burette.

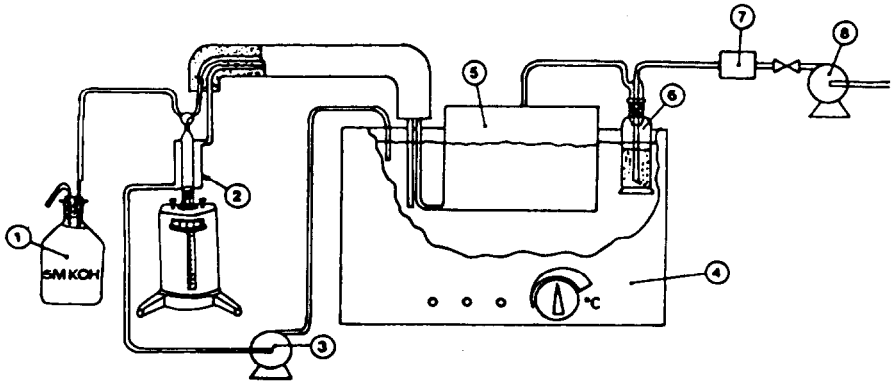

Fig. 4. Meniscus cell: (1) electrolyte container; (2) piston burette for level control; (3) pump; (4) thermostat bath; (5) meniscus cell; (6) gas scrubber; (7) gas-flow meter, and (8) gas supply.

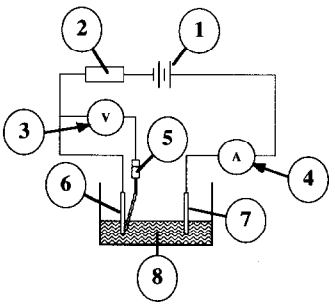

Fig. 5. Electrical system of the meniscus cell: (1) power supply; (2) resistor; (3) voltmeter; (4) ammeter; (5) reference electrode (Hg/HgO); (6) working electrode; (7) counter electrode, and (8) electrolyte (5 M KOH).

Gas to the cell is scrubbed with electrolyte in a wash bottle to humidify and remove carbon dioxide. The cell, the piston burette, and the wash bottle are kept at 40 °C.

The electrical system of the cell is shown in Fig. 5.

Electrodes

Three types of single layer test electrodes (no diffusion layer) were used:

(i) 'Nickel screen–immersion'. Electrode on nickel screen with the screen completely covered by the catalyst layer, Fig. 6.

(ii) 'Nickel plate–immersion'. Electrode on nickel plate with 5 mm from the edge of the plate covered by the catalyst layer with the rest of the plate hydrophobized with PTFE. The electrodes were immersed as in case (i). The electrode structure is shown in Fig. 6.

(iii) 'Nickel plate–cutting'. As in case (ii) with the catalyst layer successively cut away in 1 mm strips.

After the preparation process, described in the Appendix, the electrodes were mounted in the electrode holder, shown in Fig. 7. The holder was placed in the test cell and electrolyte supplied to the cell until the level indicators signaled contact. At

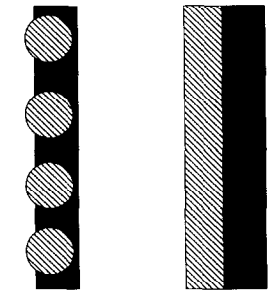

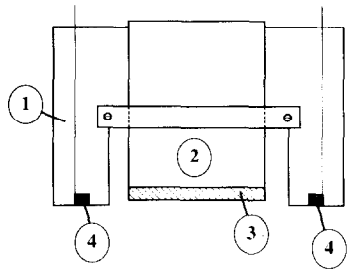

Fig. 6. Structure of electrodes supported on nickel screen and nickel plate.

Fig. 7. Electrode holder with electrode: (1) electrode holder; (2) nickel screen or plate; (3) sample, and (4) level indicators for indication of the electrolyte level.

this moment the electrolyte level is 3.0 mm below the lower edge of the electrode. The electrolyte level is then raised to the desired degree of immersion of the electrode.

The measurements were carried out with pure oxygen and with mixtures of 20.0, 5.0 and 1.0% oxygen in nitrogen. The electrodes were immersed to the desired depth-of-immersion in the electrolyte and conditioned in this position for 1 h before the electrochemical measurements.

Reproducibility

The electrode itself is a major source of variability. In fact, the meniscus approach lends itself to cost-efficient evaluation of electrode uniformity for quality control. The preparation parameters were controlled carefully, such as the number of roller passes and the pressure of compaction. The bond between the electrode layer and the nickel plate is a major source of error with the solid backing electrodes. Such problems were encountered especially in the nickel plate-cutting experiments.

The precision of the immersion parameter is estimated to be ± 0.05 mm, which corresponds to an error of about ± 1.0 mV in the recorded potential at 1 mm depth-of-immersion for a current of 1.0 mA for 6.0 cm meniscus length.

Results

The meniscus test is quite simple, which is its great advantage. On the other hand, the physical environment in the meniscus zone is quite complex with current being generated also in zone above the level of the electrolyte surface and current consumed below this level. The supporting structure for the catalyst layer, e.g., a screen, also influences the mass-transfer processes. The purpose with the three test electrode designs is to get some hints regarding these factors. There is also a possibility of modifying the experimental setup for tests with unsupported catalyst layers which would require catalyst layers with a high intrinsic conductivity, however.

The first series of experiments were carried out with electrodes with screen backing. The extended zone above the undisturbed electrolyte surface seemed to contribute a

great deal to the current generation in these tests. To decrease this effect, electrodes with nickel plate backing were prepared with the part above the test strip hydrophobized with PTFE.

Another reason for using a solid backing is that the experimental conditions resemble the '041' configuration. The solid backing setup furthermore gives the advantage of an undisturbed catalyst layer (see Fig. 6).

Figure 8 shows current–voltage curves for an electrode supported on a nickel screen. Deviations between duplicate runs are in general of the order of 5 mV. This is to be considered a fairly good reproducibility.

The curves in Fig. 9 were obtained from an electrode sample supported on a nickel plate with stepwise immersion. Figure 10 gives curves that were recorded for an electrode initially immersed to 5 mm and then slices of 1 mm was gradually cut from the lower edge of the electrode.

Figure 11 exhibits current–voltage curves for different oxygen concentrations. Theoretically, if there were only diffusional and chemical reaction resistances and no ohmic resistance [8], the current generated at a specific polarization should increase linearly with the oxygen concentration. A fivefold increase in the oxygen partial pressure, however, produces a current increase with a factor 3.4 at −183 mV versus Hg/HgO and 2.4 at −428 mV versus Hg/HgO, Fig. 11. Obviously there is a significant ohmic contribution to the overall polarization in this test.

Discussion

The characteristics of the curves exhibited in Figs. 8–11 indicate different electrode properties. The performance of gas-diffusion electrodes is strongly affected by the pretreatment of carbon and the PTFE content [9], Figs. 8 and 9. The curve for 5 mm depth-of-immersion, shown in Fig. 9, is about 160 mV better than the corresponding

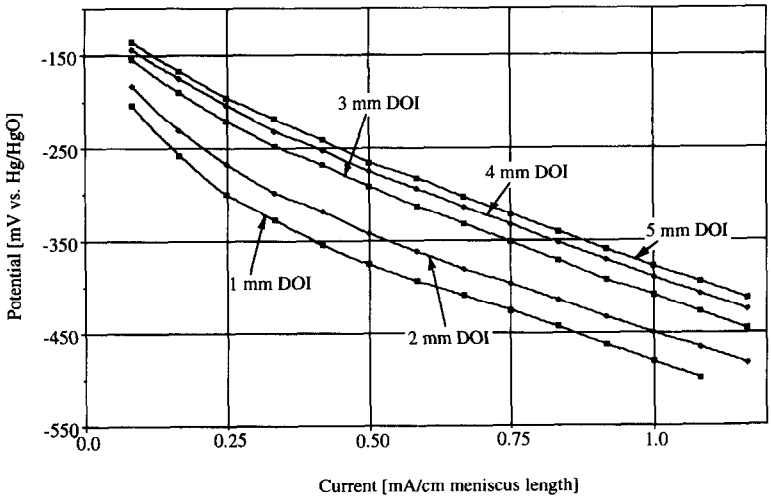

Fig. 8. Current–voltage curve for air electrode on nickel screen, 'immersion' electrode no. 74111, with 40% PTFE, untreated carbon (Shawinigan), and silver catalyst; electrode thickness: 0.5 mm. DOI = depth-of-immersion.

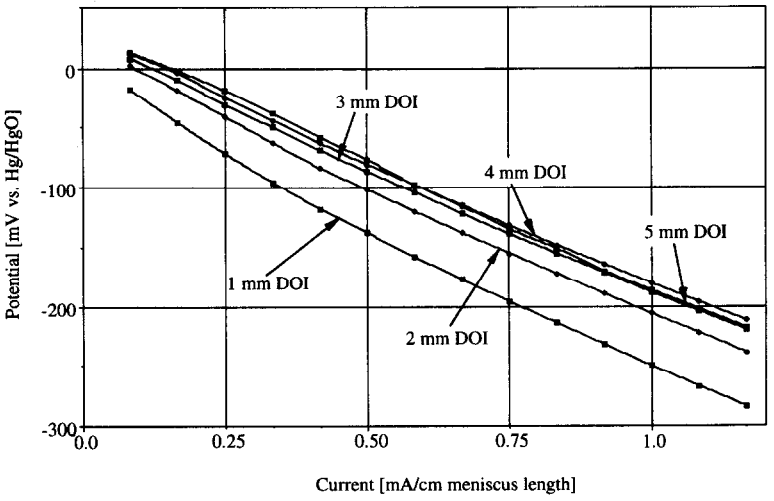

Fig. 9. Current–voltage curve for air electrode on nickel plate, 'immersion' electrode no. 74133 with 30% PTFE, acid-treated carbon (Shawinigan), and silver catalyst; electrode thickness: 0.43 mm. DOI = depth-of-immersion.

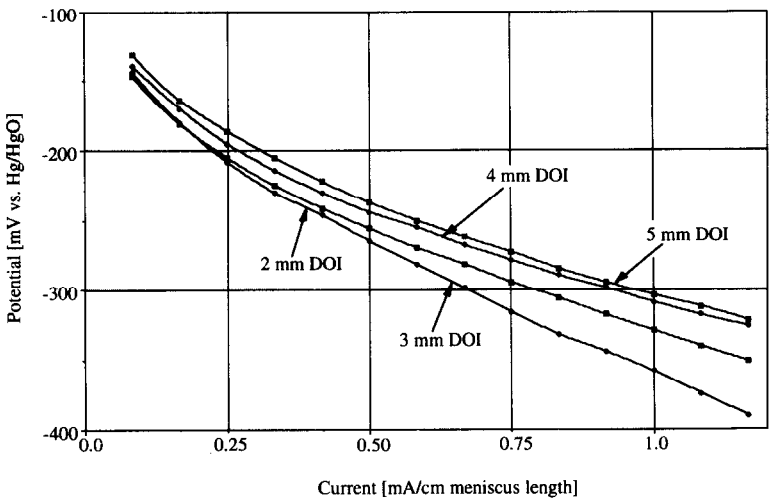

Fig. 10. Current–voltage curves for air electrode, 'cutting' electrode no. 74134 with 30% PTFE, untreated carbon (Shawinigan), and silver catalyst; electrode thickness: 0.33 mm. DOI = depth-of-immersion.

curve in Fig. 8 at a current of 1.0 mA and even larger at heavier current drains. Pretreatment of the carbon apparently has a beneficial effect.

Current–voltage curves

The current–voltage curves in Figs. 8 to 11 exhibit the same general pattern as those obtained in a conventional half-cell setup with the gas on one side and the electrolyte on the other side of the electrode. The linear parts of these curves run

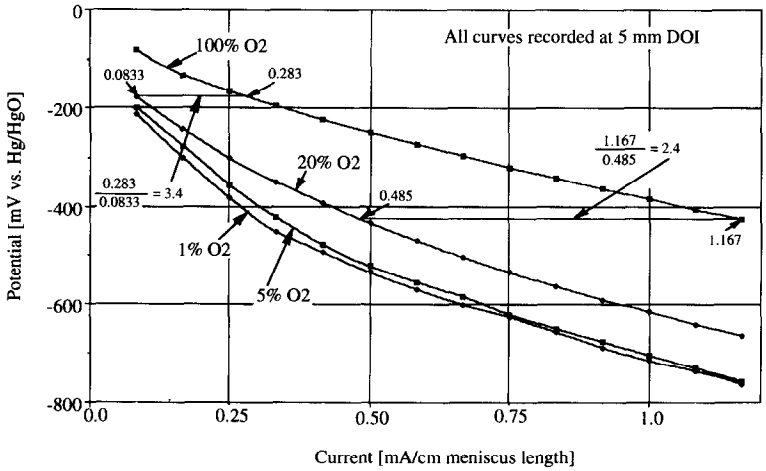

Fig. 11. Current–voltage curves for air electrode, constant immersion electrode no. 74143 with 20% PTFE, untreated carbon (Shawinigan), and silver as catalyst; electrode thickness: 0.14 mm. DOI = depth-of-immersion.

essentially in parallel, which may be interpreted so that the pseudo-resistances in this load region are not influenced by the depth-of-immersion. Intercepts on the ordinate axis differ, however. The slope of the linear parts of these curves may then be obtained by immersion of the electrode to a sufficient depth, say around 10 mm, where no further increase in electrode capacity is taking place.

The slope of the parallel curves in Figs. 8 to 11 has the dimension Ω cm, same as for specific resistivity. Apparently this 'specific resistivity' is constant and independent of the depth-of-immersion in the load range concerned here.

A very much simplified model will be used for reduction of the experimental data to produce a figure-of-merit. The current recorded for a certain depth-of-immersion is here considered to be the sum of contributions from the series of 'engaged 1 mm strips' below the electrolyte level down to the specified depth-of-immersion.

The hypothesis is here that the contribution from each strip is inversely proportional to the distance that the reactant gas has to travel from the electrolyte level to the strip in question. The performance of the meniscus electrode is thus assumed to be governed by an apparent 'specific resistance', which is constant and independent of the depth-of-immersion as illustrated in Fig. 12. This apparent resistance is denoted R (Ω), relating to the 1 mm height of a single strip. In this simplified lump model the current is assumed to be generated in the middle of each strip. The total current, I_{sum} (mA), is the sum of the contributions generated in each engaged strip.

There is uncertainty regarding the conditions in the immediate vicinity of the electrolyte level, where, in other words, the depth-of-immersion approaches zero. There could be a negative contribution to the total current, e.g., with less electrolyte film in the electrode in this area — or — an additional contribution from the area above the electrolyte level, in other words at a 'negative depth-of-immersion'.

This hypothesis is formulated in eqn. (1) where I_0 represents the contribution near the electrolyte level:

$$I_{sum} = \frac{Ult}{\rho} \sum_{\nu=1}^{n} \left[\frac{1}{\Delta x(\nu - 0.5)} \right] + I_0 \qquad (1)$$

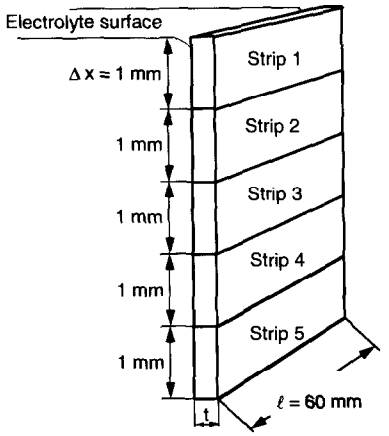

Fig. 12. Electrode immersed to 5 mm depth.

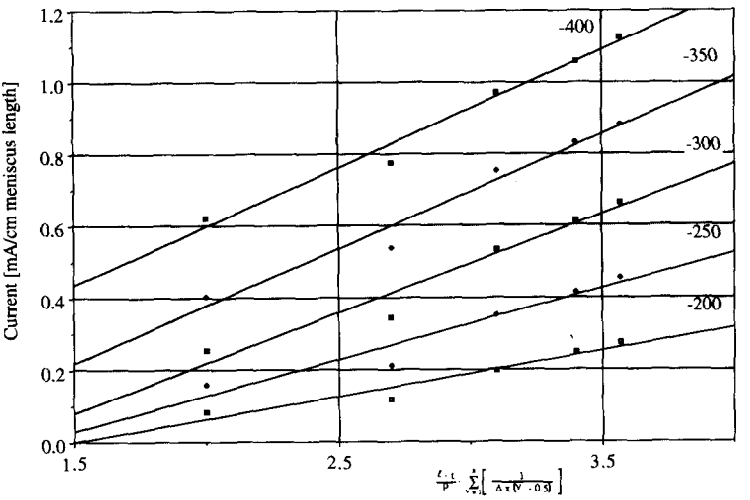

Fig. 13. Current plot vs. the term $lt/\rho\Sigma_{\nu=1}^{n}[1/\Delta x(\nu-0.5)]$.

where, I_{sum} = total current generated (mA); U = potential (mV); ρ = specific resistance (Ω cm); n = number of 1 mm strips; I_0 = contribution from meniscus zone (mA); Δx = height of strip (cm); (l) = length of strip (cm), and t = thickness of strip (cm).

Figure 13 shows a plot of I_{sum} versus $lt/\rho\Sigma_{\nu=1}^{n}[1/\Delta x(\nu-0.5)]$, based on data reported in Fig. 8. Slopes are here obtained in mV. Straight lines are obtained, which thus supports the hypothesis put forward above.

The model is admittedly quite simple but works satisfactory for the present purpose. In view of the efficient reduction of experimental data it is tempting to derive a more sophisticated model for analysis of electrode kinetics by means of data from measurements with the meniscus cell. This is not within the scope of the present work, however.

In Fig. 14, the slopes from Fig. 13 are plotted versus the associated voltage difference versus the reference electrode such as indicated in Fig. 13. In Fig. 14, the

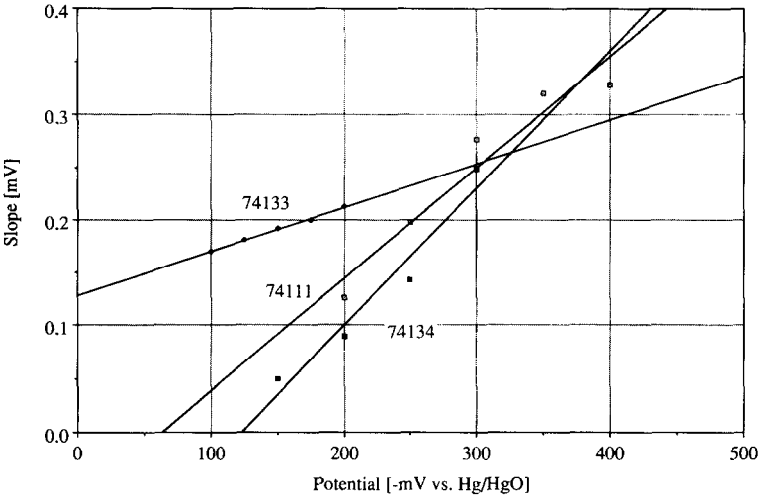

Fig. 14. Slopes from Fig. 13 plotted against the potential vs. Hg/HgO.

result of the calculation is shown for electrode no. 74111. The same calculations are made for the electrodes, nos. 74133 and 74134 (Figs. 9 and 10). These data are also plotted in Fig. 14. These curves also seem to indicate a linear relationship between the slope and the applied voltage, thus supporting the hypothesis of a constant resistivity along the immersed part of the electrode. The inverted values of the slopes in Fig. 14 may then be considered as a kind of figure-of-merit.

Apparently the processes occurring in the immediate vicinity of the electrolyte level should not influence this figure-of-merit as derived. Such phenomena may be quite important for meniscus electrodes, like Hersch's oxygen sensor, but would not be present in 'around the corner' situations.

Conclusions

The results from the measurements imply that:

1. The meniscus cell characteristics depend on the depth-of-immersion.
2. The cell could be used for quality control in electrode preparation.
3. The current–voltage curves can be transformed into figures-of-merit for the electrode and are not influenced by the effects of the meniscus zone.

Appendix

Preparation of carbons

The carbon blacks were used untreated or treated with boiling concentrated nitric acid. Acid boiling makes the surface of the carbon more hydrophilic [10–12] and reduces the fraction of submicron pores. In this study, the carbon was pretreated by boiling in concentrated nitric acid for 4 h. The carbon was then washed with distilled water. The carbon was dried and ground in a mill.

Preparation of catalysts

Silver [13] and pyrolysed cobalttetramethoxyphenylporphyrine (CoTMPP) [14] served as catalysts in these electrodes. Silver was dispersed on the carbons by the method described by Tseung and Wong [13]. The carbons were impregnated with an yaqueous solution of silver nitrate, followed by drying and heat treatment.

Preparation of electrodes

The catalyst layer must contain non-wetted gas pores as well as electrolyte-filled agglomerates where the electrochemical reaction takes place. The oxygen diffuses in the gas-filled pores to dissolve in the electrolyte in the electrolyte-filled pores of the catalyst layer [15, 16]. A electrode structure suitable for these processes is obtained in the preparation process. Several methods for the preparation of electrodes are presented in the literature [9–11, 17]. In this study the electrodes were prepared by the rolling method, originally developed by Schautz and coworkers [9, 18] and then further developed by Kiros and Schwartz [19] at the Royal Institute of Technology and by Kivisaari *et al.* [20] at the Helsinki University of Technology.

The electrodes were made of acetylene black (Shawinigan or Vulcan XR-72), Du Pont Teflon-resin 30 N (wet method) or Hostaflon TF 2053 (dry method) and a catalyst, Fig. 15.

The compounds were mixed. The powder, which was obtained, was ground and dispersed in Shellsol D-70. The dispersion was filtered. The filter cake, the 'dough', was then rolled to an electrode with a specified thickness. For the screen electrode the whole piece of screen (60 mm×80 mm) was covered by the catalyst layer. After rolling, the electrode was pressed, dried and sintered in a nitrogen atmosphere at 320 °C for 20 min.

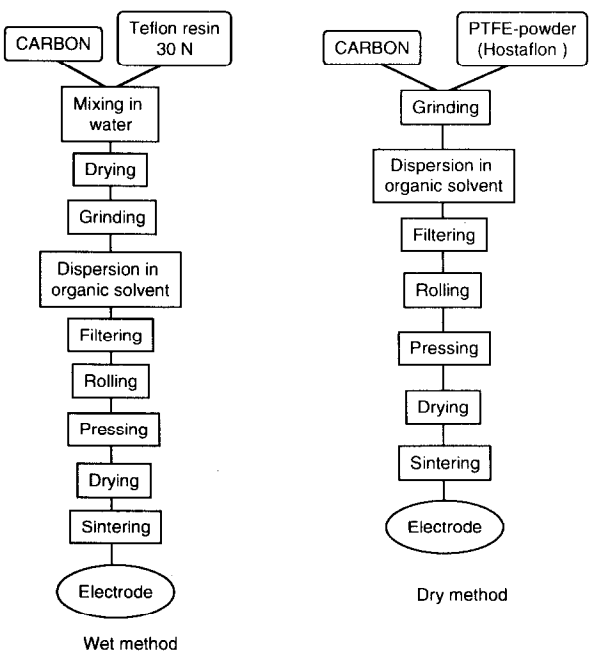

Fig. 15. Preparation of electrodes.

References

1 O. Lindström, T. Nilsson, M. Bursell, C. Hörnell, G. Karlsson, C. Sylwan and B. Åhgren, *13th Intersociety Energy Conversion Engineering Conf., San Diego, CA, USA, 1978.*
2 O. Lindström, T. Nilsson, M. Bursell, C. Hörnell, G. Karlsson, C. Sylwan and B. Åhgren, in J. Thompson (ed.), *Power Sources 7,* Academic Press, New York, 1979, pp. 419–436.
3 P. Björnbom, *Ext. Abstr., Int. Seminar, Fuel Cell Technology and Applications, Scheviningen, Netherlands, Oct. 26–29, 1987.*
4 F.G. Will, *J. Electrochem. Soc., 110* (1963) 145–160.
5 A. Kaisheva, I. Iliev and S. Gamburzev, *J. Appl. Electrochem., 9* (1979) 511–515.
6 P.A. Hersch, *US Patent No. 3 223 608.*
7 J.G. Cohn, personal communication, Stockholm, Sept. 1992.
8 P. Björnbom and J. Kivisaari, *1988 Fuel Cell Seminar, Long Beach, CA, USA, Oct. 23–26, 1988.*
9 K. Kordesch, S. Jahangir and M. Schautz, *Electrochim. Acta, 29* (1984) 1589–1596.
10 S. Motoo, M. Watanabe and N. Furuya, *J. Electroanal. Chem., 160* (1984) 351–357.
11 M. Watanabe, M. Tozawa and S. Motoo, *J. Electroanal. Chem., 183* (1985) 391–394.
12 K. Kinoshita, *Carbon, Electrochemical and Physicochemical Properties,* Wiley, New York, 1988, pp. 199–200.
13 A.C.C. Tseung and L.L. Wong, *J. Appl. Electrochem., 2* (1972) 211–215.
14 O. Lindström, E. Björnbom and T. Kaimakis, *Annual Meet. Symp. Fuel Cells IV, San Francisco, CA, USA, Nov. 5–10, 1989,* American Institute of Chemical Engineers, New York.
15 A.D.S. Tantram and A.C.C. Tseung, *Nature, 221* (1969) 167–168.
16 P. Björnbom, *J. Electrochem. Soc., 133* (1986) 1874–1875.
17 B.J. Krätschmer, Untersuchung von Kohlenmaterialien für Gasdiffusionselektroden, *Thesis,* University of Graz, 1981, pp. 15–22.
18 M. Schautz, Herstellung von Elektroden für alkalische Wasserstoff-Luft-Brennstoffzellen und Bau einer Batterie, *Thesis,* University of Graz, 1984, pp. 54–58.
19 Y. Kiros and S. Schwartz, *1990 Fuel Cell Seminar, Phoenix, AZ, USA, Nov. 25–28, 1990.*
20 J. Kivisaari, J. Lamminen, M.J. Lampinen and M. Viitanen, *J. Power Sources, 32* (1990) 233–241.